



Aging and Environmental Effects on the Superconductor

$[Y_{1-x}Ca_x]SrBaCu_{2.80}(BO_3)_{0.20}O_y$ with $0.10 \leq x \leq 0.50$

A. G. Bustamante Dominguez¹ · H. E. Sanchez Cornejo¹ · J. C. González¹ · G. M. Ingo² · C. Riccucci² · G. Di Carlo² · M. Pascucci² · J. Albino Aguiar³ · C. H. W. Barnes⁴ · L. De Los Santos Valladares^{3,4}

Received: 29 March 2024 / Accepted: 11 April 2024 / Published online: 22 May 2024
© The Author(s) 2024

Abstract

The long-term (more than 20 years) aging effect and degradation study of a $[Y_{1-x}Ca_x]SrBaCu_{2.80}(BO_3)_{0.20}O_y$ powder ceramic superconductors with $0.10 \leq x \leq 0.50$ are studied by X-ray diffraction and DC Magnetic Property Measurement System (DC-MPMS-SQUID). The samples prepared by solid state reaction were well characterized and stored at normal conditions of pressure and temperature for more than 20 years. The aged samples present the formation of $BaCO_3$ due to the exposure with the environment during that period. The temperature dependence of the magnetization under $H_{ext} = 10$ Oe reveal that the superconducting state remains in the samples, except for that with $x = 0.10$, where a higher magnetic field (20 kOe) is required to be applied to observe a superconducting response. Remarkably, the samples show the same T_C values despite the aging indicating that the magnetic alignment of the formed $BaCO_3$ affects the magnetic properties of the whole sample but not the superconducting alignment of the doped YBCO. This is also reflected in the $\chi^{-1}(T)$ plots at normal state, which show both ferromagnetic and antiferromagnetic contribution, in contrast to what was obtained in the pristine samples which only presented antiferromagnetic coupling. From $M(H)$ loops, the critical current density values at 10 K are obtained by using the critical Bean model in order to estimate the transport capabilities of the aged powders.

Keywords Aging effect · YBCO superconductor · High- temperature superconductors · Cuprates · Borates

1 Introduction

Currently, among the various limitations to be solved during the development of superconducting materials, there are still pending tasks to overcome such as achieving temporal stability of superconductivity behavior at several experimental

conditions [1], getting vortex creep [2], and avoiding the aging effect and environmental degradation [3–7]. In particular, it is well known that the superconductivity property of cuprate superconductors degrades or destroys with time [8]. Thus, understanding the aging effect of the cuprate superconductors is vital for industrial applications.

Among high critical temperature cuprate superconductors (HTSC), $YBa_2Cu_3O_7$ (YBCO) is one of the most studied and promising for industrial applications. Previous studies about the aging effect on YBCO reports that it reacts with surrounding air if the sample is kept unprotected for a long time. This leads to the degradation of the superconducting properties [9]. Nonetheless, at relative short-time, the YBCO does not show any major change in ambient air [10]. For long-term applications it is important to protect any device made from YBCO superconductor by coating or controlling the surrounding atmosphere.

On the other hand, double-site-doped YBCO with rare earths or lanthanides has been extensively studied for both, understanding the origin of the superconductivity and to increase the T_C in YBCO. In particular, studies about YBCO

✉ A. G. Bustamante Dominguez
abustamanted@unmsm.edu.pe

✉ L. De Los Santos Valladares
ld301@cam.ac.uk

¹ Laboratorio de Cerámicos y Nanomateriales, Facultad de Ciencias Físicas, Universidad Nacional Mayor de San Marcos, Calle Germán Amézaga 375, Lima, Peru

² Istituto per lo Studio dei Materiali Nanostrutturati, CNR-Montelibretti, Rome, Italy

³ Programa de Pós-Graduação em Ciência de Materiais, Universidade Federal de Pernambuco, Av. Jorn. Aníbal Fernandes, s/n, CEP 50670-901 Recife, PE, Brazil

⁴ Cavendish Laboratory, Department of Physics, University of Cambridge, J.J. Thomson Ave., Cambridge CB3 0HE, UK

doped with Ca and BO_3 : $[\text{Y}_{1-x}\text{Ca}_x]\text{SrBaCu}_{2.80}(\text{BO}_3)_{0.20}\text{O}_7$ with $0.10 \leq x \leq 0.50$ has been demonstrated that the superconducting transition occurs at $T_C = 77$ K, being this value independent of the calcium content [11].

However, there is lack of information about the aging effect in double-site-doped YBCO such as $[\text{Y}_{1-x}\text{Ca}_x]\text{SrBaCu}_{2.80}(\text{BO}_3)_{0.20}\text{O}_7$ with $0.10 \leq x \leq 0.50$ which could provide information about the stability of the bonding between doped rare earth and ions into the YBCO structure with time. The present work reports the changes occurred in the crystalline structure and superconducting properties in $[\text{Y}_{1-x}\text{Ca}_x]\text{SrBaCu}_{2.80}(\text{BO}_3)_{0.20}\text{O}_7$ powder samples due to the aging effect for more than 20 years.

2 Experimental

The pristine superconducting samples were prepared in 2000 by following the solid-state reaction method [11]. In brief, stoichiometric amounts of Y_2O_3 , BaO_2 , SrCO_3 , CaCO_3 , CuO , and H_3BO_3 were grinded and sintered at 1273 K for 16 h in air and O_2 . The pristine samples were characterized and then stored under normal laboratory environmental conditions for 24 years.

The crystallization of the aged samples was studied by X-ray diffraction (XRD) technique. The data were collected from 8 to 80° (0.01° step) using a powder universal diffractometer Bruker D8 with $\text{Cu K}\alpha_1$ radiation ($\lambda = 1.54056 \text{ \AA}$). The crystallite size was estimated from the basic Scherrer's formula, neglecting peak broadening caused by residual stresses in the films [12].

$$D = \frac{K\lambda}{\beta_{hkl} \cos \theta_{hkl}} \quad (1)$$

where D is the average crystallite size, λ is the wavelength of the applied X-ray ($\lambda_{\text{Cu-K}\alpha_1} = 0.154056 \text{ nm}$), θ_{hkl} is the Bragg's angle, β_{hkl} is the width of the x-ray peak on the 2θ axis, which can be easily found by measuring the full width at the half maximum (FWHM) of the reflection, and K is the so-called Scherrer Constant. K depends of the crystallite shape and the size distribution, indices of the diffraction line, and the actual definition used for β whether FWHM or integral breadth [13]. K can have values from 0.62 and 2.08. In the present work, $K = 0.916$ is used.

The powder diffraction patterns were refined using the Rietveld refinement method using the FullProf Suite program (January 2021 version). The background of the powder X-ray diffraction was refined using a linear interpolation between a set of background points with refinable heights. A pseudo-Voigt function [14] was used to describe the reflection profiles. No corrections for absorption or micro-absorption were applied. The R values (R_p , R_{wp} , R_{exp} , R_{Bragg} ,

and R_F) as well as the S parameter were used as numerical convergence criteria for the refinement. The definition of the R parameters is described in reference [15]. To ensure the convergence of the structural parameters, the Rietveld refinement was performed following the order described in reference [16].

Temperature dependence of the magnetization was measured by using a Quantum Design DC Magnetic Property Measurement System (DC-MPMS-SQUID) magnetometer equipped with a 7-T superconducting magnet. The data were collected in zero field cooling (ZFC) and field cooling (FC) modes at applied magnetic fields from 10 Oe and 20 kOe for superconducting and normal state, respectively. The magnetization hysteresis loops were measured using the same DC-MPMS-SQUID equipment. All the $M(H)$ measurements were done under applied magnetic fields from -5 to $+5$ T and at 10 K.

Critical current density J_C values were estimated using the critical state Bean model, according to the relation between the irreversible magnetization M_{irr} and J_C (see Eq. (2)) [17]:

$$J_C = \left[\frac{30\Delta M}{d} \right] \quad (2)$$

where M^+ and M^- are the magnetization branches in the fully penetrated state for decreasing and increasing applied fields, respectively, and $\Delta M = M^- - M^+$. The unit of ΔM is emu/cm^3 , and d is the crystallite diameter of each superconducting sample.

3 Results and Discussion

Figure S1 shows the XRD pattern for each sample with $0.1 \leq x \leq 0.5$ for the Ca composition. The presence of the peaks (103), (104), (113), (200), (116), (220), and (310) corresponds to the superconductor phase, in agreement with the XRD pristine samples [11]. Additionally, carbonate barium BaCO_3 reflections were detected, being its presence product of the interaction between the samples and the environment along the years. However, the presence of BaCO_3 reflections is not clearly observed in the sample with $x = 0.3$. As complement for the XRD characterization for the aged samples, some SEM micrographs together with their respective EDX analysis are presented in Fig. S2. Regarding the carbon presence, Tables S1–S5 reveal C in all the aged samples, corroborating the presence of BaCO_3 .

The Rietveld refinement of the two series is shown in the Fig. 1. The raw data were analyzed in the tetragonal structure with $P4/mmm$ symmetry by Rietveld refinement technique to obtain the structural parameters. At the initial stage of refinements for the main phase of YBCO, it is assumed

Fig. 1 Rietveld refinement of XRD patterns (in logarithmic scale) of the **a** pristine and **b** aged $[Y_{1-x}Ca_x]SrBaCu_{2.80}(BO_3)_{0.20}O_7$ with $0.10 \leq x \leq 0.50$ samples

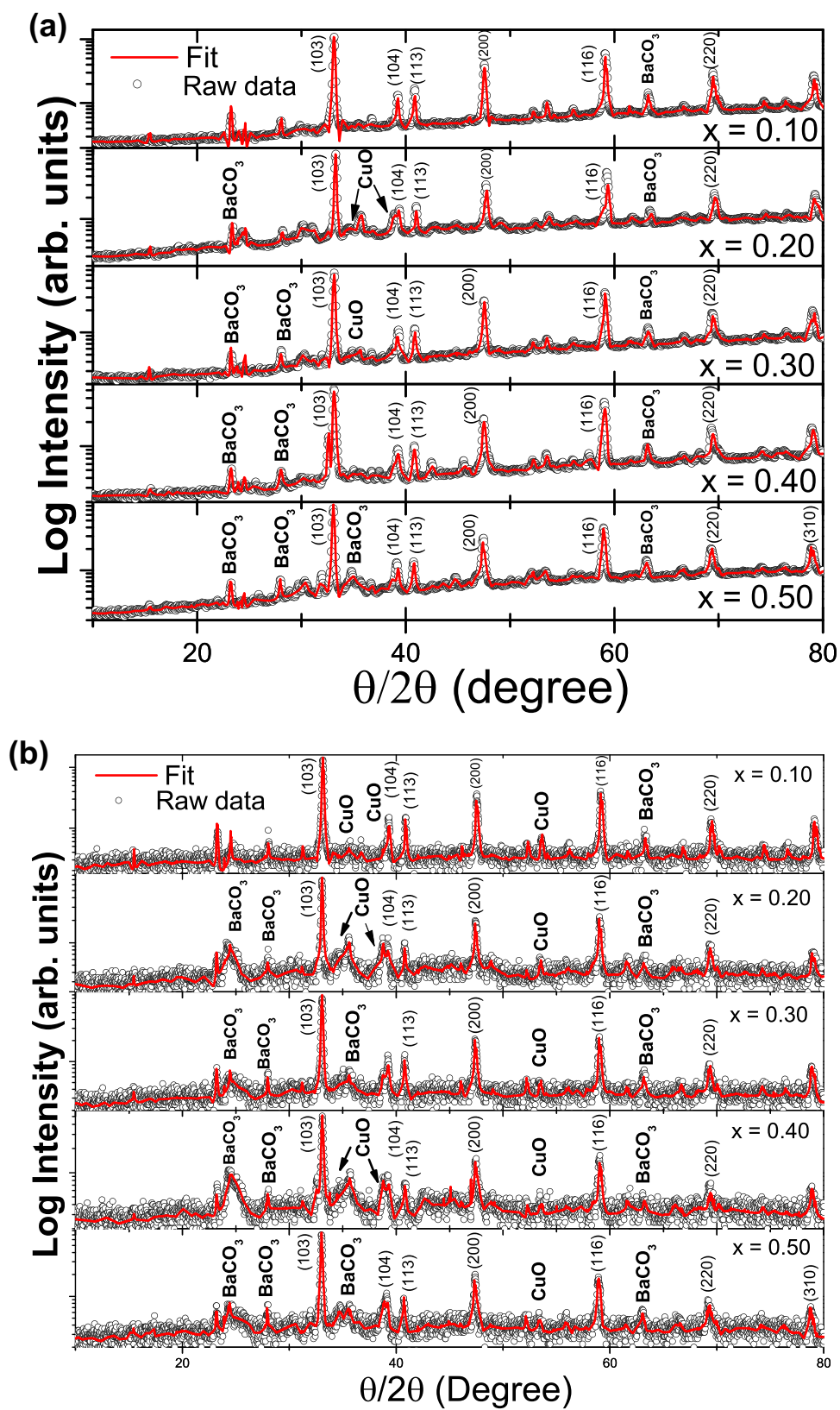


Table 1 Refined structural parameters for the pristine $[Y_{1-x}Ca_x]SrBaCu_{2.80}(BO_3)_{0.20}O_7$ with $0.10 \leq x \leq 0.50$ samples

Fractional coordinate	$x = 0.10$	$x = 0.20$	$x = 0.30$	$x = 0.40$	$x = 0.50$
z_{Ba}	0.18610	0.18317	0.18350	0.18518	0.18517
$z_{Cu(2)}$	0.35740	0.35140	0.35702	0.35856	0.36243
$z_{O(2)}$	0.37820	0.37185	0.35011	0.36669	0.35670
$z_{O(3)}$	0.15730	0.16060	0.16989	0.18169	0.18062
$x_{O(4)}$	0.20021	0.20021	0.20021	0.20021	0.20021
$z_{O(4)}$	0.09390	0.09390	0.09390	0.09390	0.09390
$x_{O(5)}$	-0.3500	-0.35000	-0.35000	-0.35000	-0.35000
Content					
Y	0.68752	0.66447	0.64887	0.55596	0.46015
Ca	0.31248	0.33553	0.35113	0.44404	0.53985
Cu(1)	0.80000	0.80277	0.78808	0.80310	0.78529
B	0.20000	0.19723	0.21192	0.19690	0.21471
O(1)	0.30000	0.65443	0.71066	0.66436	0.61741
O(4)	0.12500	0.10708	0.48754	0.29260	0.05374
O(5)	0.12500	0.07754	0.41962	0.29264	0.05374
R and S values					
R_{wp}	28.50	44.7	35.20	31.20	29.30
R_{exp}	11.76	16.95	17.95	16.40	16.31
R_p	39.70	70.50	57.50	55.10	49.70
R_{Bragg}	14.57	21.64	16.04	12.46	11.54
R_F	12.60	18.42	17.48	15.44	16.67
S	5.97	6.97	3.84	3.62	3.23

that the occupancies for the sites Ba ($1/2, 1/2, z_{Ba}$), Cu(2) ($0, 0, z_{Cu(2)}$), O(2) ($0, 0, z_{O(2)}$), and O(3) ($0, 0, z_{O(3)}$) are all set to 1. The Ca atom was assumed to occupy at Y-site. Also, the

oxyanion BO_3 was assumed to occupy at Cu(1) site. Oxygen atoms were assumed to occupy at O(1), O(2), O(3), O(4), and O(5) sites. The oxygens O(4) and O(5) were employed to

Table 2 Refined structural parameters for aged $[Y_{1-x}Ca_x]SrBaCu_{2.80}(BO_3)_{0.20}O_7$ with $0.10 \leq x \leq 0.50$ samples

Fractional coordinate	$x = 0.10$	$x = 0.20$	$x = 0.30$	$x = 0.40$	$x = 0.50$
z_{Ba}	0.18499	0.18504	0.18792	0.18907	0.18724
$z_{Cu(2)}$	0.36399	0.36104	0.36343	0.36645	0.36370
$z_{O(2)}$	0.35244	0.34291	0.35406	0.35179	0.34252
$z_{O(3)}$	0.22446	0.26837	0.22590	0.26232	0.18714
$x_{O(4)}$	0.20021	0.20021	0.20021	0.20021	0.20021
$z_{O(4)}$	0.09390	0.09390	0.09390	0.09390	0.09390
$x_{O(5)}$	-0.3500	-0.3500	-0.3500	-0.3500	-0.3500
Content					
Y	0.84815	0.77017	0.66031	0.61099	0.49032
Ca	0.15186	0.22983	0.33969	0.38901	0.50968
Cu(1)	0.80192	0.80626	0.80361	0.80000	0.80351
B	0.19808	0.19374	0.19639	0.20000	0.19649
O(1)	0.69895	0.66700	0.50000	0.66816	0.66349
O(4)	0.10554	0.17008	0.02703	0.15969	0.47048
O(5)	0.11616	0.17008	0.40987	0.22623	0.08483
R and S values					
R_{wp}	45.70	61.80	50.40	62.30	72.30
R_{exp}	34.92	51.74	44.30	53.26	63.45
R_p	63.0	119.0	81.90	117.0	148.0
R_{Bragg}	15.05	28.59	13.28	19.49	19.92
R_F	15.14	19.97	15.14	19.96	22.15
S	1.71	1.43	1.29	1.37	1.30

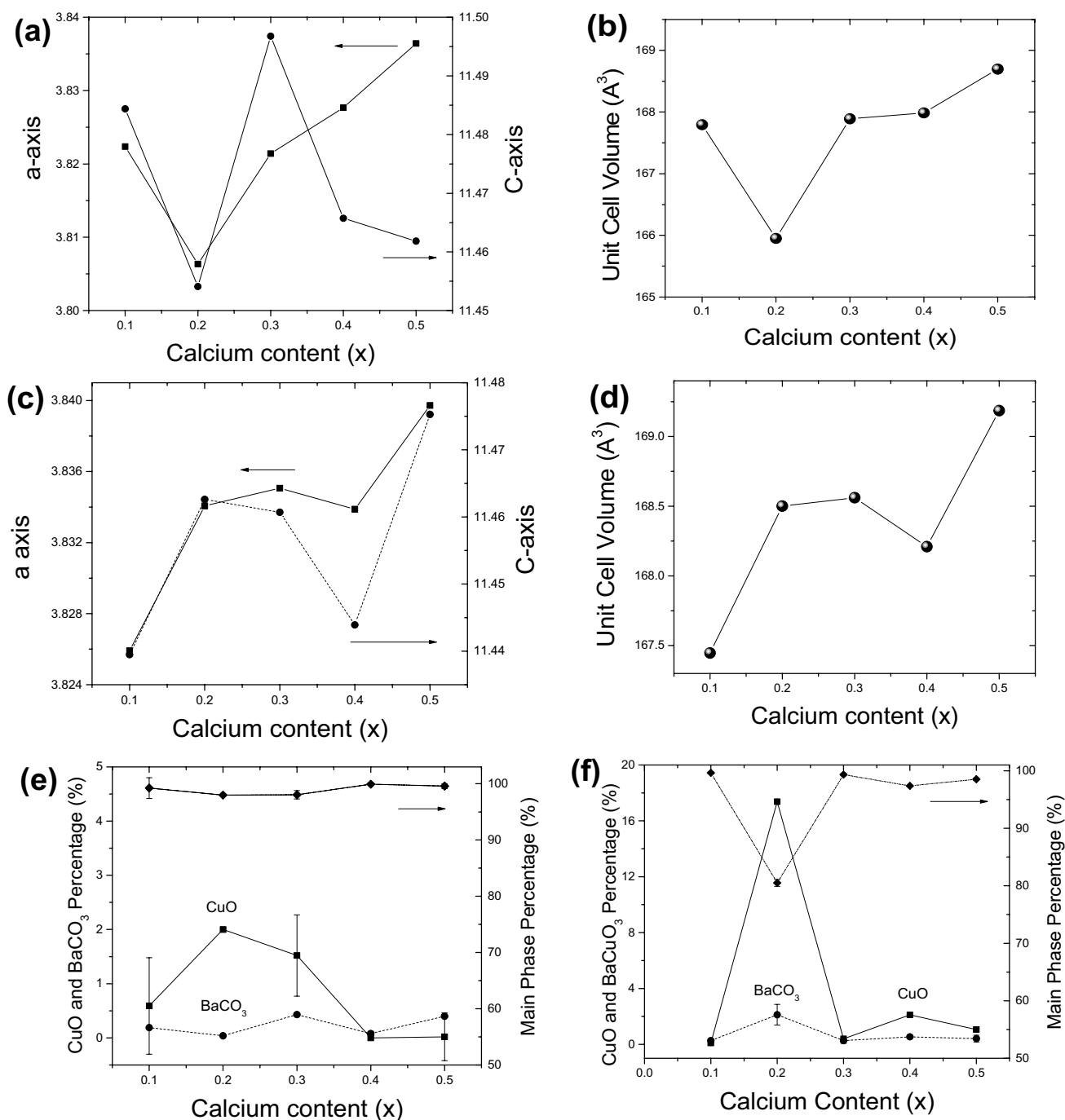


Fig. 2 a, b Lattice parameters of the pristine sample. c, d Lattice parameters of the aged samples. e, f CuO and BaCO₃ spurious phase percentage in pristine and aged $[Y_{1-x}Ca_x]SrBaCu_{2.80}(BO_3)_{0.20}O_7$ with $0.10 \leq x \leq 0.50$ samples, respectively

link the B atom. Moreover, the occupancies of oxygen atoms sited at O(1), O(4), and O(5) were refined. The fractional coordinates oxygen atoms sited at O(4) and O(5) were inaccurate due to the weak X-ray scattering power for oxygen atoms. For this reason, the fractional coordinates were fixed. The structural parameters for the samples were refined so that the calculated pattern fits the observed one very well.

A summary of the refined atomic parameters for both series is given in Tables 1 and 2.

The lattice parameters versus Ca content, x , are plotted in Fig. 2 for the pristine and the aged samples. Due to the ionic radii of the calcium atom (0.99 Å) being bigger than the yttrium atom (0.93 Å), the cell unit volume increases as more calcium atoms enter the structure replacing the yttrium

atom. This increase is also observed in the cell parameters like a - and c -axes despite the difference in the ionic between calcium and yttrium; calcium (Ca^{2+}) has a lower valence value than yttrium (Y^{3+}). This fact is exposed in the cell unit volume where the valence reaches the balance with $x=0.20$ for the pristine samples (Fig. 2b) and $x=0.40$ for aged samples (Fig. 2d). The jumps observed in the lattice parameters is caused by the competition between two local inner stress in the unit cell, ionic radii, and atom valence. Moreover, CuO and BaCuO_3 spurious phase percentage in the pristine and aged samples is shown in Fig. 2e, f, respectively. These two phases were found in a major percentage in the aged samples than in the pristine ones.

With the aim of quantify the aging and environmental effect in the superconducting properties, Fig. 3 shows the temperature dependence of the zero-field cooling susceptibility in the two samples series. Figure 3a shows a clear diamagnetic response measured under applied magnetic field of 10 Oe for the $x=0.20, 0.30, 0.40,$ and 0.50 of the aged samples, with $T_c=75.33, 75.30, 79.40,$ and 73.35 , respectively. These T_c values are obtained from the $d\chi/dT$ curves shown in the inset of Fig. 3a. Despite the long time, it does not show appreciable changes compared with the non-aged samples (see Fig. 3c) [11]. According to Fig. 3a, the sample with Ca concentration $x=0.1$ does not show diamagnetic signal and therefore does not exhibit the superconducting phenomena. However, at temperatures below 10 K, the susceptibility values decay, which suggests that there is a diamagnetic component in the sample. The ZFC χ vs. T plot at under a higher magnetic field, 20 kOe, is shown in Fig. 3b. Interestingly, under this H_{ext} , the powder with $x=0.10$ shows diamagnetic response, corresponding to the superconducting behavior, similar to the $x=0.10$ pristine sample. However, under the same applied field, the curve corresponding to the Ca-content $x=0.5$ begins to lose its superconductor response. This might indicate that the value of the applied H_{ext} is close to the H_{c2} and thus the superconductivity is destroyed. In addition, the presence of the CuO and BaCO_3 secondary phases affects the superconducting transition, as noted by comparing Fig. 3a and b. This is clearly distinguished at low T in both cases, which arise in a positive contribution signal. For the pristine samples, the diamagnetic signal reaches saturated values for all Ca content.

Figure 4 shows the temperature-dependence of the inverse magnetic DC susceptibility in the normal state, at the temperature range 100 to 300 K and under $H_{\text{ext}}=20$ kOe. The plots show a typical Curie-Weiss behavior in all the cases. However, for $x=0.3$ and 0.4 in the aged samples (see Fig. 4a), two (positive and negative) θ_c values are discovered, indicating two (ferromagnetic and antiferromagnetic) coupling contributions. Since the pristine samples showed only antiferromagnetic coupling under the same applied magnetic field [11], the aging

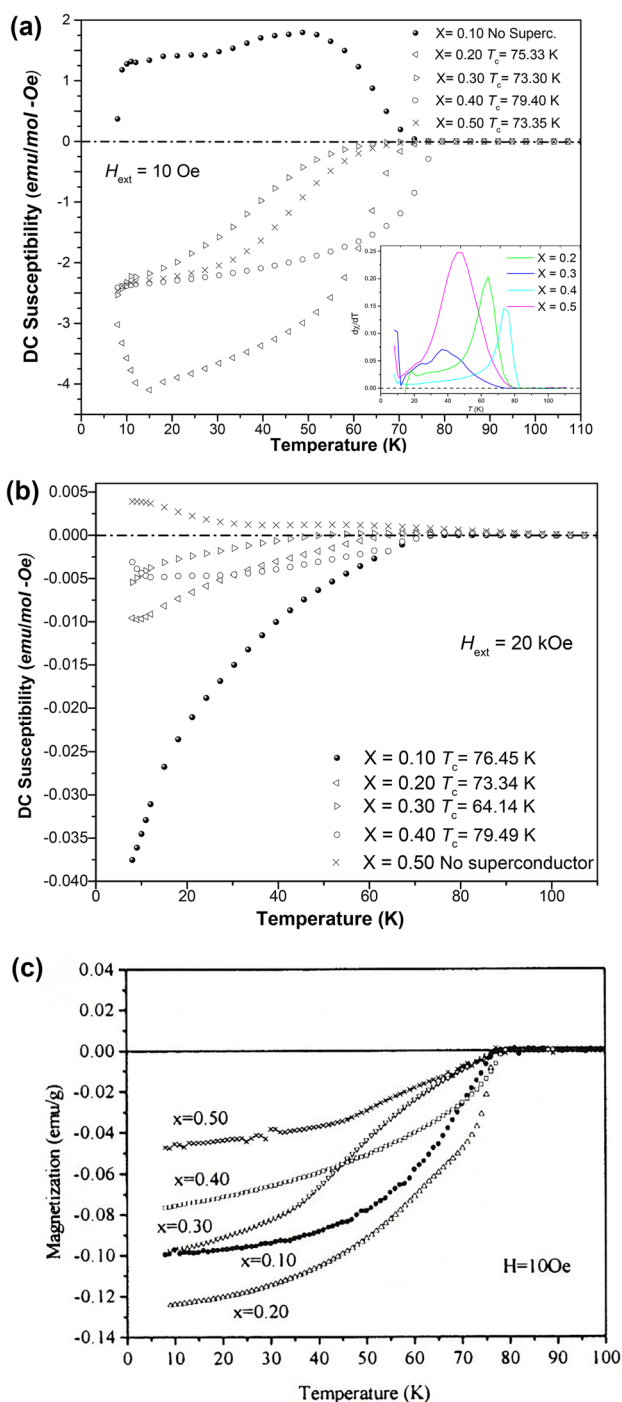
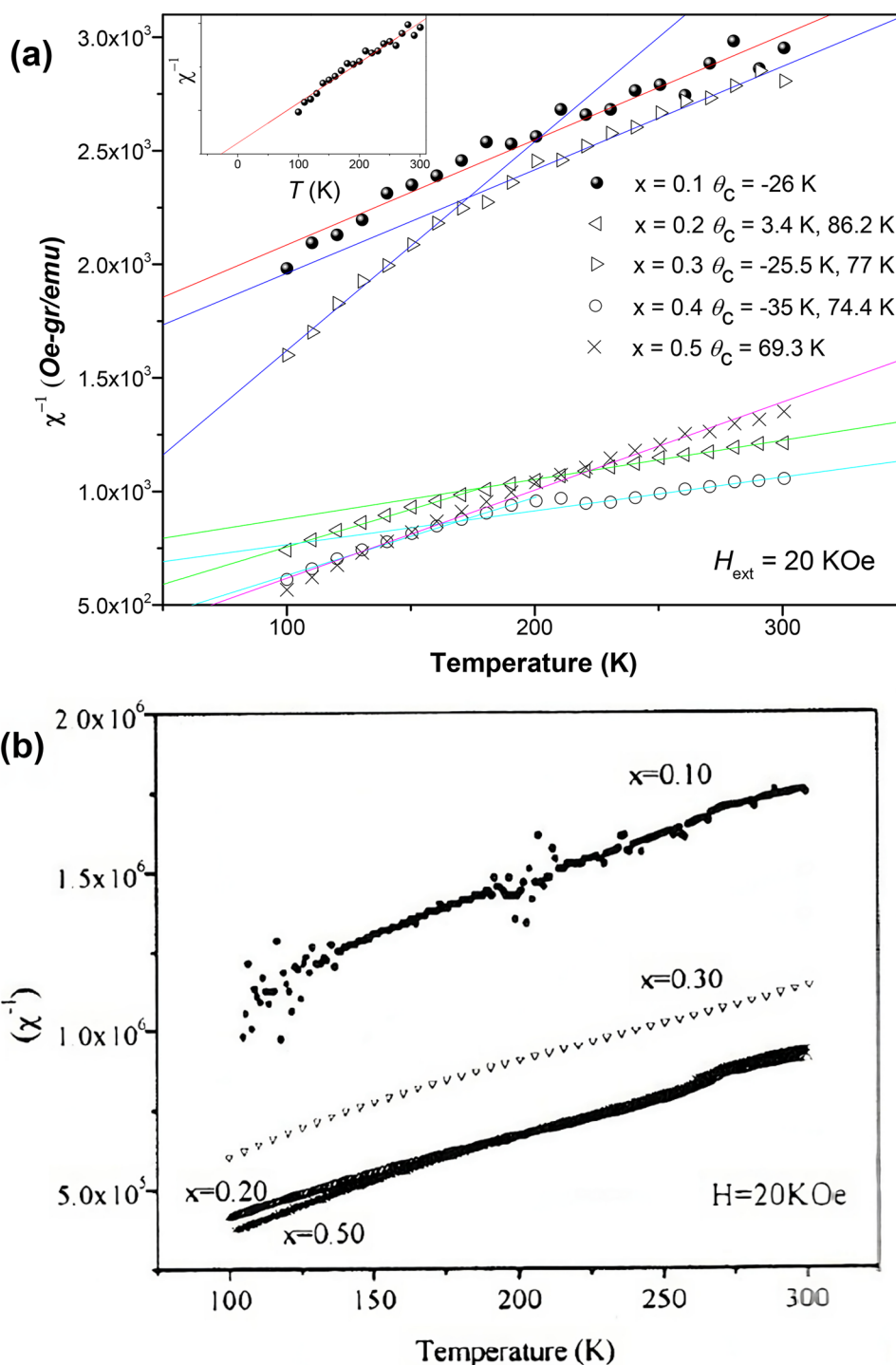


Fig. 3 Zero-field cooling DC susceptibility vs. temperature plots under a 10 Oe applied field **a** and 20 kOe **b** for the aged samples, and under 10 Oe for the pristine samples **c**. **c** Reprinted from reference [11] with permission from Elsevier

effect has produced the appearance of a ferromagnetic signal. For $x=0.2$ and 0.5 , the new coupling observed corresponds to ferromagnetic with positive θ_c values. Table 3 summarizes the T_c and θ_c values found for the two series samples.

Fig. 4 Inverse magnetic DC susceptibility versus temperature plots measured at $H_{ext} = 20$ kOe for the aged **a** and pristine samples **b**. All the plots show a typical Curie-Weiss behavior. **b** Reprinted from reference [11] with permission from Elsevier



To check if the aged samples are suitable for potential application, the critical current density $J_C(H)$ isothermal curves were indirectly estimated from the hysteresis loops (see Fig. 5a) by using the Bean model. Figure 5b shows the J_C values for each aged powder at 10 K. The results indicate that for $x = 0.1$, J_C reaches the highest values (around 10^6

A/cm²) at 10 K ($\mu_0 H_{ext} = 0.5$ T). However, for all cases, a rapid decay of the J_C values is observed. Nevertheless, considering its age, these presented J_C values indicate that the samples are suitable for potential application. The presence of the carbonate barium ($BaCO_3$) does not affect the transport capabilities of the studied samples.

Table 3 A comparison of the characteristic temperatures at normal (θ_c) and superconducting (T_c) state for the pristine and aged-doped YBCO powder samples

Ca content	Pristine samples		Aged samples		
	θ_c (K)	T_c (K) (at 10 Oe)	θ_c (K)	T_c (K) (at 10 Oe)	T_c (K) (at 20 kOe)
$X=0.1$	-255.28	≈ 77	-26.00	No supercond	76.45
$X=0.2$	-93.36		3.40; 86.20	75.33	73.34
$X=0.3$	-191.48		-25.50; 77.00	73.30	64.14
$X=0.4$	-79.02		-35.00; 74.40	79.40	79.49
$X=0.5$	-62.18		69.30	73.35	No supercond

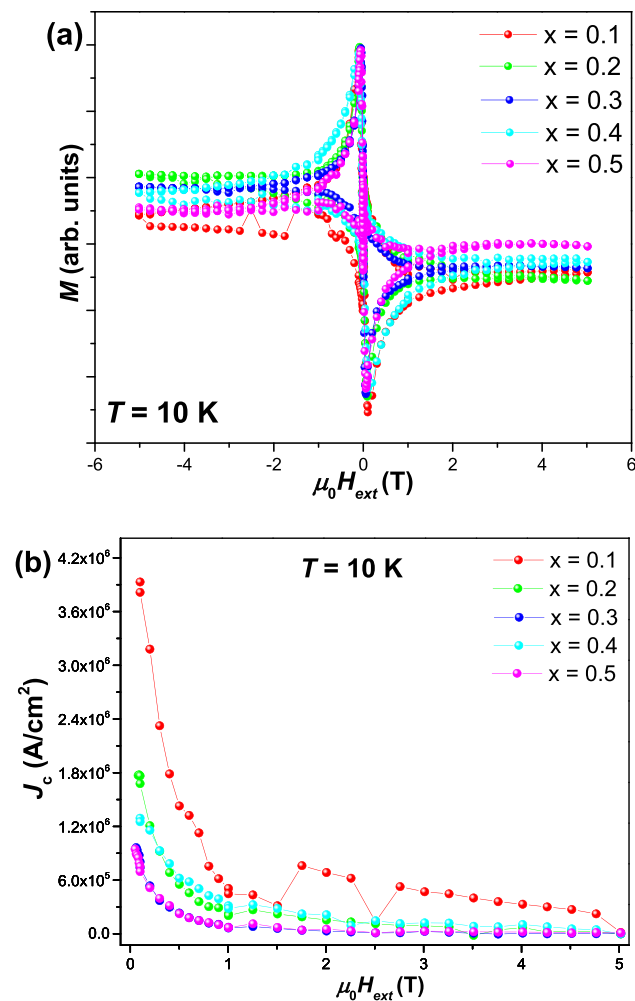


Fig. 5 **a** Hysteresis loops measurements at 10 K for the aged samples. **b** Critical current density values estimated by using the critical Bean model in the $M(H)$ loops

4 Conclusions

The aging effect in $[Y_{1-x}Ca_x]SrBaCu_{2.80}(BO_3)_{0.20}O_y$ powder samples stored for 20 years at normal conditions of pressure and temperature was studied. The structural characterization, made by XRD and Rietveld refinement,

revealed that barium carbonate $BaCO_3$ has been formed during the stored period. This is corroborated by SEM-EDS that shows the presence of carbon in all the EDS spectra and on several sites. The aging and environmental effect in the superconducting properties was studied by temperature dependence of the zero-field cooling susceptibility plots under 10 Oe and 20 kOe applied magnetic fields. The powders show superconducting behavior in agreement with the pristine samples 24 years ago without any appreciable change of T_c . Critical current density values were estimated by the critical Bean model, evidencing that despite the morphological degradation, the samples still present J_c potentially applicable values. Overall, the presence of the formed $BaCO_3$ should have affect the superconducting properties of the sample.

Supplementary Information The online version contains supplementary material available at <https://doi.org/10.1007/s10948-024-06745-2>.

Acknowledgements A. G. B. D thanks the CNR for supporting his visiting to the Istituto per lo Studio dei Materiali Nanostrutturati, Montelibretti, Rome, Italy.

Author Contribution Data acquisition, methodology, data curation, and formal analysis: A. Bustamante Dominguez, H. Sanchez Cornejo, and L. De los Santos Valladares; conceptualization, interpretation, validation, data curation, and visualization: H. Sanchez Cornejo, A. Bustamante Dominguez, J. C. González, G.M. Ingo, C. Riccucci, G. Di Carlo, M. Pascucci, J. Albino Aguiar, C.H.W. Barnes, and L. De Los Santos Valladares; and all authors have contributed in writing and reviewing the manuscript.

Funding This work has been supported by the Peruvian Agency of Science CONCYTEC-PROCIENCIA through grants No. PE501082724-2023-PROCIENCIA and No PE501082814-2023-PROCIENCIA. The work in the UK has been supported by the Cambridge Royce facilities grant CAM-YR8-UI-009-REAS. The work in Brazil has been supported by the PROFESSOR VISITANTE Program No. 13/2022 of the Universidade Federal de Pernambuco, Brazil, Contract No. 062/2022 (Process no. 23076.101469/2021-69).

Data Availability No datasets were generated or analyzed during the current study.

Declarations

Competing Interests The authors declare no competing interests.

Open Access This article is licensed under a Creative Commons Attribution 4.0 International License, which permits use, sharing, adaptation, distribution and reproduction in any medium or format, as long as you give appropriate credit to the original author(s) and the source, provide a link to the Creative Commons licence, and indicate if changes were made. The images or other third party material in this article are included in the article's Creative Commons licence, unless indicated otherwise in a credit line to the material. If material is not included in the article's Creative Commons licence and your intended use is not permitted by statutory regulation or exceeds the permitted use, you will need to obtain permission directly from the copyright holder. To view a copy of this licence, visit <http://creativecommons.org/licenses/by/4.0/>.

References

1. Cornejo, H.S., De Los Santos Valladares, L., Barnes, C.H., Moreno, N.O., Domínguez, A.B.: Texture and magnetic anisotropy of $\text{YBa}_2\text{Cu}_3\text{O}_{7-x}$ film on MgO substrate. *J. Mater. Sci. Mater. Electron.* **31**, 21108–21117 (2020). <https://doi.org/10.1007/s10854-020-04623-w>
2. Malozemoff, A.P.: Flux creep in high temperature superconductors, *Physica C: Superconductivity Volumes 185–189. Part. 1*, 264–269 (1991). [https://doi.org/10.1016/0921-4534\(91\)91983-B](https://doi.org/10.1016/0921-4534(91)91983-B)
3. Siddiqi, S.A., Pirzada, Z.M., Mateen, A.: Aging and environmental effects on $\text{YBa}_2\text{Cu}_3\text{O}_{6.95}$ superconductor. *JMEP* **4**, 212–215 (1995). <https://doi.org/10.1007/BF02664115>
4. Bustamante, A., De Los Santos Valladares, L., Flores, J., Barnes, C.H., Majima, Y.: Aging effect in $\text{CaLaBa}\{\text{Cu}_{1-x}\text{Fex}\}_3\text{O}_{7-\delta}$ with $0 \leq x \leq 0.07$ studied by Mössbauer spectroscopy. *Hyperfine Interact.* **203**, 119–124 (2011). <https://doi.org/10.1007/s10751-011-0371-z>
5. Lanoël, L., Rozas, G., Bruchhausen, A.E., Amigó, M.L., Ale Crivillero, M.V., Hofer, J.A., Villafuerte, M., Bridoux, G., Bengió, S., Nieva, G.: Effects of aging processes at the surface of the superconductor $\beta\text{-FeSe}$. *Phys. Rev. B.* **106**, 214507 (2022). <https://doi.org/10.1103/PhysRevB.106.214507>
6. Nikoghosyan, S.K., Harutyunyan, V.V., Baghdasaryan, V.S., Mughnetyan, E.A., Zargaryan, E.G., Sarkisyan, A.G.: The effect of aging on the superconducting transition temperature and resistivity of Y-Ba-Cu-O ceramics after high temperature treatment. *IOP Conf. Ser. Mater. Sci. Eng.* **49**, 012042 (2013). <https://doi.org/10.1088/1757-899X/49/1/012042>
7. Lee, S., Jang, J., Jung, H.S., Kang, W.N., Lee, S.Y.: Effects of ageing on the microwave surface resistance of MgB2 superconductor films stored in low vacuum. *Electron Mater. Lett.* **15**, 572–581 (2019). <https://doi.org/10.1007/s13391-019-00157-4>
8. Svoboda, P., Vašek, P., Smrčková, O., Plecháček, V., Nevřiva, M.: Aging effects in ceramic high- T_C superconductors. *Solid State Commun. Commun.* **75**(4), 331–334 (1990). [https://doi.org/10.1016/0038-1098\(90\)90906-R](https://doi.org/10.1016/0038-1098(90)90906-R)
9. Hussain, A., Sayer, M.: Aging effects on the superconducting properties of Y-Ba-Cu oxide films. *Vacuum* **43**(12), 1195–1196 (1992)
10. Schlesier, K., Huhtinen, H., Granroth, S., Paturi, P.: An aging effect and its origin in GdBCO thin films. *J. Phys. Conf. Ser.* **234**, 012036 (2010). <https://doi.org/10.1088/1742-6596/234/1/012036>
11. Bustamante Domínguez, A.G., Barinotto, V.-H.C., Flores Santibañez, J., Garcia, F.: Phase formation and superconductivity in $[\text{Y}_{1-x}\text{Ca}_x]\text{SrBaCu}_{2.80}(\text{BO}_3)_{0.20}\text{O}_y$ with $0.10 \leq x \leq 0.50$. *Physica C.* **341**, 635–636 (2000). [https://doi.org/10.1016/S0921-4534\(00\)00625-0](https://doi.org/10.1016/S0921-4534(00)00625-0)
12. Cullity, B.D.: In: *Elements of X-ray diffraction*, pp. 96–102. Addison-Wesley Publishing Company Inc, USA (1956)
13. Langford, J.I., Wilson, A.J.C.: Scherrer after sixty years: a survey and some new results in the determination of crystallite size. *J. Appl. Cryst.* **11**, 102–113 (1978). <https://doi.org/10.1107/S0021889878012844>
14. Young, R.A., Wiles, D.B.: Profile shape functions in Rietveld refinements. *J. Appl. Cryst.* **15**, 430–438 (1982). <https://doi.org/10.1107/S002188988201231X>
15. Young, R.A.: Introduction to the Rietveld method. In: Young, R.A. (ed.) *The Rietveld method*. Oxford University Press, United Kingdom (1993)
16. Gonzalez, J.C., Lándinez, D.A., Albino Aguiar, J., Bustamante, A.: Structural refinement of $[\text{Y}_{1-x}\text{Ca}_x]\text{SrBaCu}_{2.80}(\text{PO}_4)_{0.20}\text{O}_y$. *Physica C.* **354**, 375–378 (2001). [https://doi.org/10.1016/S0921-4534\(01\)00104-6](https://doi.org/10.1016/S0921-4534(01)00104-6)
17. Eley, S., Miura, M., Maiorov, B., Civale, L.: Universal lower limit on vortex creep in superconductors. *Nat. Mater.* **16**, 409–413 (2017). <https://doi.org/10.1038/nmat4840>

Publisher's Note Springer Nature remains neutral with regard to jurisdictional claims in published maps and institutional affiliations.